SPECTRAL ESTIMATES OF MARINE TURBULENCE.

Allan Bruce Lund

NAVAL POSTGRADUATE SCHOOL
Monterey, California

THESIS

SPECTRAL ESTIMATES OF MARINE TURBULENCE DATA

by

Allan Bruce Lund

March 1975

Thesis Advisor: Kenneth L.Davidson

Approved for public release; distribution unlimited.

SECURITY CLASSIFICATION OF THIS PAGE (When Date Entered)

REPORT DOCUMENTATION PAGE		READ INSTRUCTIONS BEFORE COMPLETING FORM
1. REPORT NUMBER	2. GOVT ACCESSION NO.	3. RECIPIENT'S CATALOG NUMBER
4. TITLE (and Subtitle) Spectral Estimates of Marine Turbulence Data		5. TYPE OF REPORT & PERIOD COVERED Master's Thesis; March 1975 6. PERFORMING ORG. REPORT NUMBER
7. AUTHOR(s) Allan Bruce Lund		8. CONTRACT OR GRANT NUMBER(s)
9. PERFORMING ORGANIZATION NAME AND ADDRESS Naval Postgraduate School Monterey, California 93940 •		10. PROGRAM ELEMENT, PROJECT, TASK AREA & WORK UNIT NUMBERS
11. CONTROLLING OFFICE NAME AND ADDRESS Naval Postgraduate School Monterey, California 93940		12. REPORT DATE March 1975 13. NUMBER OF PAGES
14. MONITORING AGENCY NAME & ADDRESS(if different from Controlling Office)		15. SECURITY CLASS. (of this report) Unclassified 15a. DECLASSIFICATION/DOWNGRADING SCHEDULE

16. DISTRIBUTION STATEMENT (of this Report)

Approved for public release; distribution unlimited.

17. DISTRIBUTION STATEMENT (of the abstract entered in Block 20, if different from Report)

18. SUPPLEMENTARY NOTES

19. KEY WORDS (Continue on reverse side if necessary and identify by block number)

20. ABSTRACT (Continue on reverse side if necessary and identify by block number)

Velocity and temperature fluctuations from multi-level measurements in the marine boundary layer were examined to determine the validity of present formulations and prediction techniques. Spectral distributions were analyzed using an analog analyzer as opposed to the digital computer methods previously utilized at the Naval Postgraduate School.

DD FORM 1 JAN 73 1473 EDITION OF 1 NOV 65 IS OBSOLETE
S/N 0102-014-6601 |
(Page 1)

SECURITY CLASSIFICATION OF THIS PAGE (When Date Entered)

In general, the height variations of the dissipation rate of turbulent kinetic energy, momentum flux, and the temperature structure parameter observed in this study agree with the over-land expressions developed by Wyngaard. Most deviations from expected results were attributed to apparent anomalies in spectral results.

It has been shown that the analog spectral analysis performed in this study produced information which is as reliable as that from digital methods.

Spectral Estimates of Marine Turbulence Data

by

Allan Bruce Lund
Lieutenant, United States Navy
B.S., University of Utah, 1967

Submitted in partial fulfillment of the
requirements for the degree of

MASTER OF SCIENCE IN METEOROLOGY

from the

NAVAL POSTGRADUATE SCHOOL
March 1975

ABSTRACT

Velocity and temperature fluctuations from multi-level measurements in the marine boundary layer were examined to determine the validity of present formulations and prediction techniques. Spectral distributions were analyzed using an analog analyzer as opposed to the digital computer methods previously utilized at the Naval Postgraduate School.

In general, the height variations of the dissipation rate of turbulent kinetic energy, momentum flux, and the temperature structure parameter observed in this study agree with the overland expressions developed by Wyngaard. Most deviations from expected results were attributed to apparent anomalies in spectral results.

It has been shown that the analog spectral analysis performed in this study produced information which is as reliable as that from digital methods.

TABLE OF CONTENTS

LIST OF TABLES

LIST OF FIGURES

ACKNOWLEDGEMENTS

Much of the credit for this thesis belongs to Dr. Kenneth L. Davidson for his patience and guidance in analyzing the data and preparation of this thesis. Special thanks to Dr. Thomas Houlihan for his indispensable aid and guidance in acquiring knowledge of the operation and calibration of the experiment equipment, especially the analog spectrum analyzer with the associated numerous recalibrations. I want to also thank Mr. Steve Rinard and Mr. Charles Leonard for assistance in the spectral analysis of the data and Professor Charles L. Taylor for photographic contributions used in this thesis.

Finally, I want to thank my wife Cathie, whose many hours of typing initial drafts and many more hours of patient understanding made this task possible.

I. INTRODUCTION

This is a study of velocity and temperature fluctuations in the marine boundary layer. The data examined were obtained from multi-level measurements with tungsten wire velocity probes and platinum wire temperature probes. The measurements were made from the Naval Postgraduate School research vessel, ACANIA. Mean wind and temperature measurements are also utilized to complement and analyze the fluctuation data. A separate investigation on the mean data has been completed by Smedley (1975).

The purpose of this study is to examine properties of small scale temperature and velocity fluctuations in the marine environment, on the basis of spectral distributions. A significant aspect of the study is that spectral distributions were obtained utilizing an analog spectrum analyzer, rather than digital computer methods. The latter has been the method used previously in atmospheric turbulence experiments at the Naval Postgraduate School. The study includes descriptions of the variation with height of (1) ε (the viscous dissipation of turbulent kinetic energy) and (2) C_T^2 (the temperature structure parameter).

II. THEORETICAL CONSIDERATIONS

A. BACKGROUND

This study is one of a continuing investigation of multiple-level overwater observations from a ship. The ship is the R/V ACANIA, shown in Figure 1, operated by the Department of Oceanography, Naval Postgraduate School. Because these were shipboard measurements, only high frequency small scale fluctuations could be measured. The following paragraphs will review the theoretical considerations used to interpret the small fluctuation data. Parallel reviews of this theory have been provided by Johnston (1974) and Bone (1974). The latter involved initial examinations of data obtained with the same instrumentation used in this study.

B. TURBULENT KINETIC ENERGY BALANCE EXPRESSION

In a simplified form, the turbulent kinetic energy balance expression for neutral conditions can be written

$$\overline{-u'w'} \frac{\partial \bar{u}}{\partial z} = \varepsilon \qquad (1)$$

where $\bar{u}$ represents the mean wind at height z and the term $\frac{\partial \bar{u}}{\partial z}$ is the wind shear. Equation (1) states that mechanical production of turbulent kinetic energy, $\overline{-u'w'} \frac{\partial \bar{u}}{\partial z}$, equals the molecular dissipation of turbulent kenetic energy, ε.

Equation (1) is often written as

$$u_*^2 \frac{\partial \bar{u}}{\partial z} = \varepsilon \qquad (2)$$

Figure 1. The R/V ACANIA

where $u_*^2 = \overline{-u'w'}$, and $\overline{-u'w'}$ represents the vertical transfer of horizontal momentum by turbulent fluctuations.

For neutral conditions in a constant stress boundary layer, the following expression is valid for the wind gradient

$$\frac{\partial \bar{u}}{\partial z} = \frac{u_*}{Kz} \tag{3}$$

where K is Von Karman's constant. Combining Equations (2) and (3) yields an expression to estimate u_* on the basis of measurements of ε at a known height z.

$$u_*^3 = \varepsilon K z \tag{4}$$

Equation (4) can be rewritten

$$\text{Ln } \varepsilon = -\text{Ln } z + \text{Ln } \frac{u_*^3}{K} \tag{5}$$

which is a form used in later analysis of the variation of ε with height.

For non-neutral conditions the turbulent kinetic energy balance expression (Garratt 1972) is

$$u_*^3 = \varepsilon K z \left(\frac{1}{\phi_m(\xi) - \xi} \right) \tag{6}$$

For an unstable case ($R_i < 0$),

$$\phi_m(\xi) = (1 - 16\ \xi)^{-\frac{1}{4}} \tag{7}$$

and $\xi = R_i$.

For the stable case ($R_i > 0$),

$$\phi_m(\xi) = 1 + 5\ \xi \tag{8}$$

and

$$\xi = \frac{R_i}{1 - 5\ R_i}$$

where R_i is the Richardson number,

$$R_i = g/\overline{T} \left(\partial T/_{\partial z}\right) / \left(\partial \overline{u} /_{\partial z}\right)^2$$

Equation (5) can be rewritten as

$$\text{Ln } \varepsilon = -\text{Ln } \left(z/_{(\phi_m(\xi) - \xi)}\right) + \text{Ln } \frac{u_*^3}{k} \qquad (9)$$

A plot of Ln ε versus the first term on the right hand side of Equations (5) or (9) would yield a straight line with -1 slope. Figure 2 illustrates the possible effects of instability on the predicted plot of Ln z versus Ln ε, where Ln $\phi_2(R_i)$ is an empirical function of the Richardson number. Deviations from this relationship could be interpreted as either due to deviations from the constant flux assumption arising from the influence of wind-wave coupling or non-neutral stratifications.

From the above discussion, ε can be used to estimate u_* values. u_* is an important parameter in boundary layer studies since it defines the intensity of turbulent transfer of momentum toward the surface. It is assumed to be constant with height in the first 30 meters.

C. SPECTRAL SIMILARITY THEORY

Kolmogorov's second hypothesis is the basis for estimating ε and C_T^2 (the temperature structure function parameter) from spectra of velocity and temperature fluctuations. It is based on similarity expressions for the inertial subrange, which is the wave number region where energy is transferred without dissipation from lower to higher wave numbers.

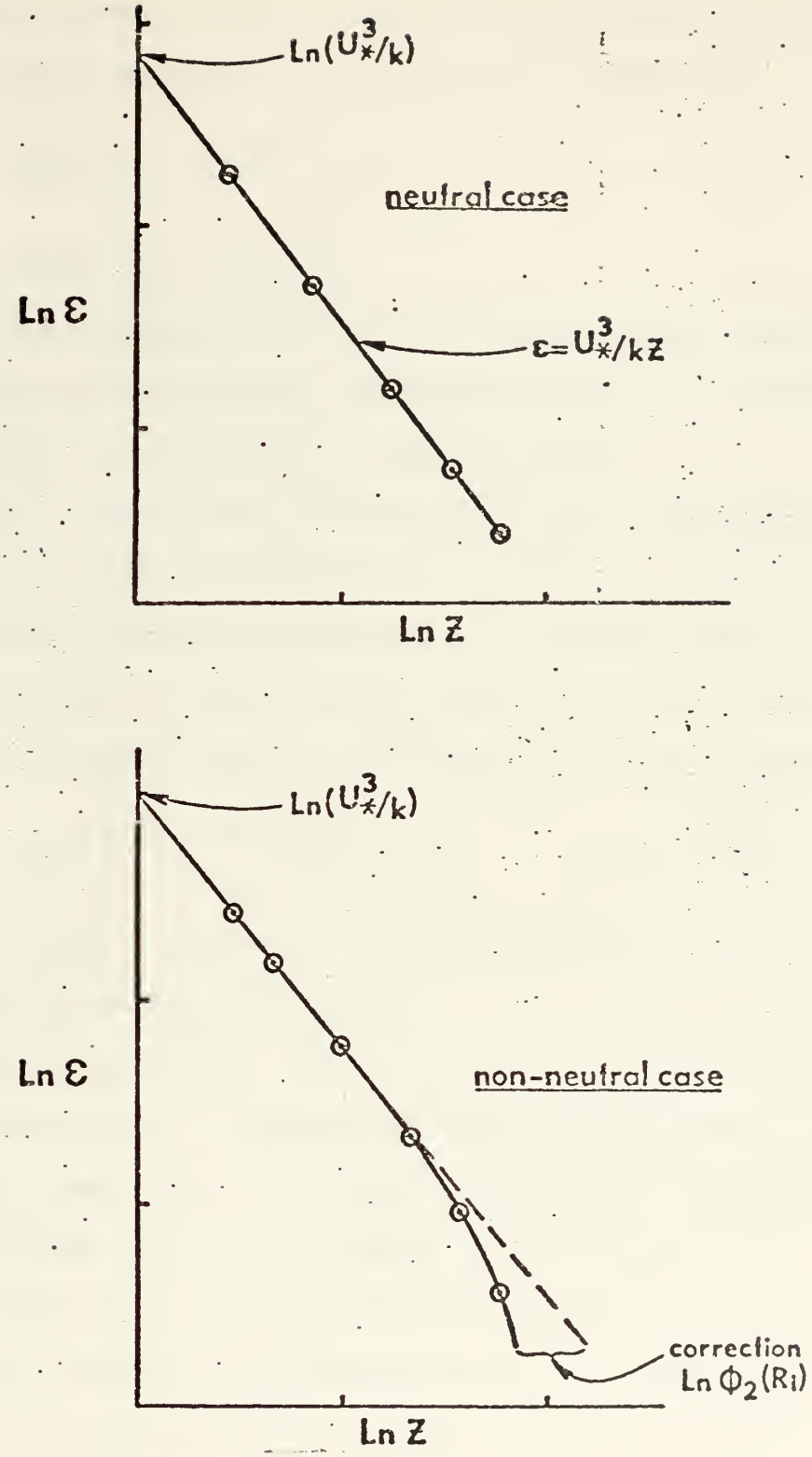

Figure 2. An Illustration of the Effect of Stability on Variation of ε with Height.

The following relationships were proposed by Kolmogorov for spectral densities in the inertial subrange,

$$\phi(k) = c_1 \varepsilon^{2/3} k^{-5/3} \tag{10}$$

$$\phi_T(k) = c_2 C_T^2 k^{-5/3} \tag{11}$$

where $\phi(k)$ and $\phi_T(k)$ are the one dimenensional spectra for velocity and temperature respectively and k is the streamwise component of wave number as defined below.

ε has already been discussed in it's relationship to u_*. Another turbulence parameter of interest in this study is the temperature-structure parameter, C_T^2, which appears in equation (11). It is important because it is related to the refractive-index-structure parameter, C_N^2, by the expression

$$C_N^2 = \left(79 \times 10^{-6} \frac{P}{T^2}\right)^2 C_T^2 \tag{12}$$

C_N^2 is a primary parameter in the characterization of optical propagation in the environment.

Height variations of C_T^2 are dependent on stability, as was the case for ε. Predicted height variations for various stability conditions are shown in Figure 3. Wyngaard, et. al. (1971), noted that C_T^2 decreased with height as $Z^{-2/3}$ for stable conditions and as $Z^{-4/3}$ for unstable conditions.

Since velocity and temperature fluctuations are measured at a fixed point in the flow, the resultant spectra are realized at a "temporal" frequency, f. To obtain an ε and C_T^2, the time (f) and space (k) scales must be related by Taylor's (1938) "frozen turbulence" hypothesis, i.e.,

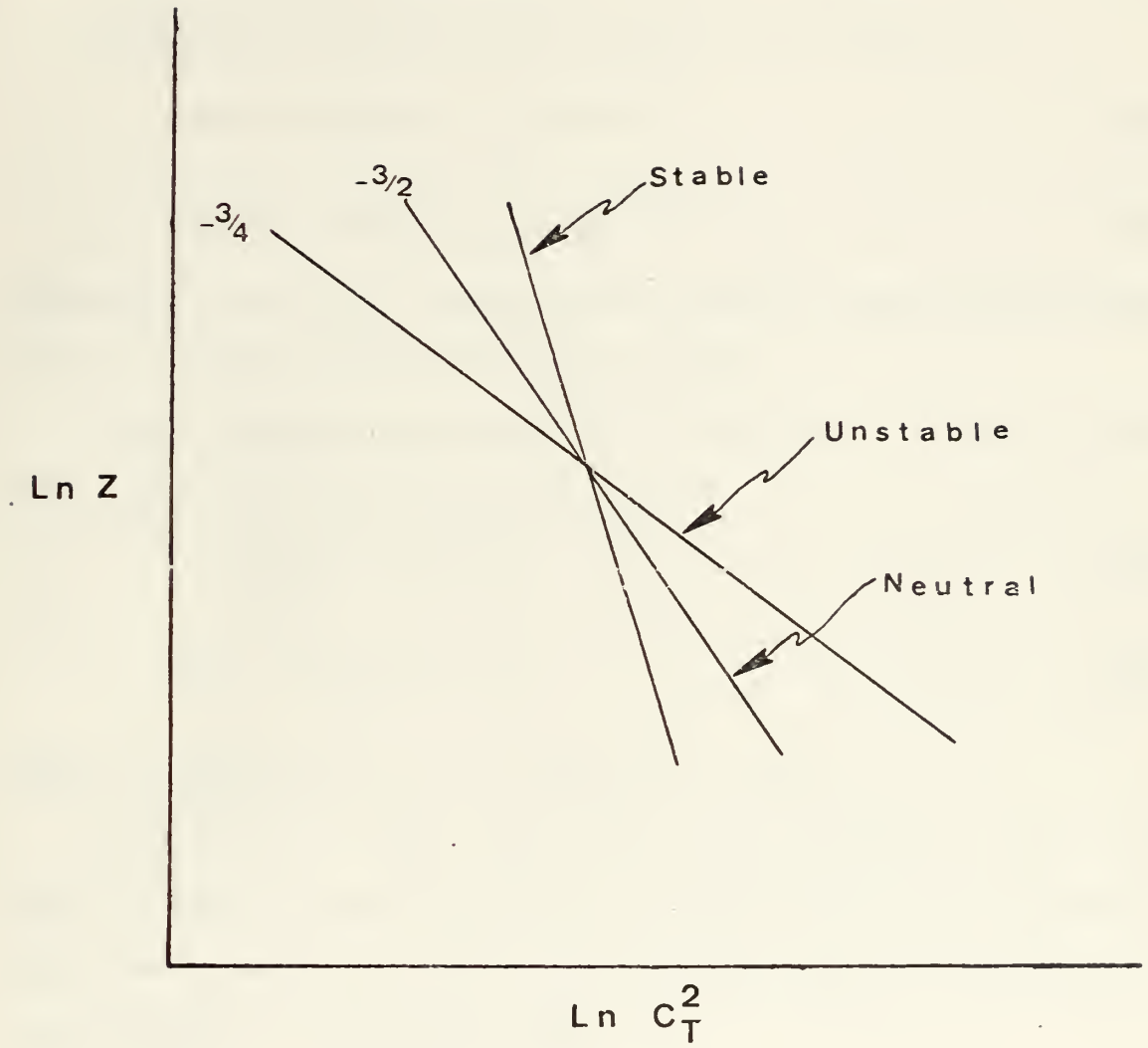

Figure 3. An illustration of the effect of stability on the variation of C_T^2 with height.

$$k = \frac{2\pi f}{\bar{u}}$$

where $\bar{u}$ is the mean wind speed at the measurement level. The term "frozen" implies the turbulence pattern remains unchanged as it sweeps past the probe.

Equations (11) and (12) can also be written as

$$f\phi(f) = k\phi(k) = c_1 \varepsilon^{2/3} k^{-2/3} \tag{13}$$

$$f\phi_T(f) = k\phi_T(k) = c_2 C_T^2 k^{-2/3} \tag{14}$$

where $\phi(f)$ and $\phi_T(f)$ are spectral density values with units of $(m/sec)^2/Hz$ and $^oC^2/Hz$ respectively.

Final forms of Equations (13) and (14), in terms of $\phi(f)$ and $\phi_T(f)$, which are measured, are

$$\varepsilon = \left(\frac{k^{2/3}}{c_1} f\phi(f) \right)^{3/2} \tag{15}$$

$$C_T^2 = \frac{k^{2/3}}{c_2} f\phi_T(f) \tag{16}$$

where, empirically, $c_1 = 0.5$ and $c_2 = 0.25$.

From Equations (15) and (16), with measured f, $\phi(f)$, $\phi_T(f)$, and $\bar{u}$, ε and C_T^2 can be determined at each level of interest. These were the final forms used to determine the variation with height of ε and C_T^2 values.

III. DATA COLLECTION AND SENSOR CALIBRATION

A. THE PLATFORM

Observations were obtained aboard the R/V ACANIA anchored off Monterey, California in Monterey Bay. Measurements were made at four levels on two masts spatially mounted on the forward deck of the ship. Figure 4 illustrates the sensor locations on these masts. Figure 5 shows the vane and probe arrangement. The vane maintained a one dimensional profile of the wind during measurements.

B. INSTRUMENTATION

The velocity fluctuation sensors were TSI model 1210 probes with sliding support shields and tungsten wires. The shields permitted isolation of the sensing region for determination of the undisturbed velocity, V_o, before and after each experiment. The platinum coated tungsten wire was small enough to resolve the viscous dissipation scale without any need to apply wire length corrections. The wire was fitted with plated ends for isolating the sensing area and thereby minimizing flow disturbance.

Electronics associated with each probe were a TSI Model 1054B Linearized Anemometer, a TSI Model 1056 Variable Decade Module and a Model 1057 Signal Conditioner. The signal conditioner was only used during the March 1974 observations. The anemometer had a linear frequency response from DC to 10

LEGEND

$\bar{u}$ Cup Anemometer
$\bar{T}$ Quartz Thermometer
$\bar{q}$ Humidiometer
u' Hot Wire
T' Platinum Wire

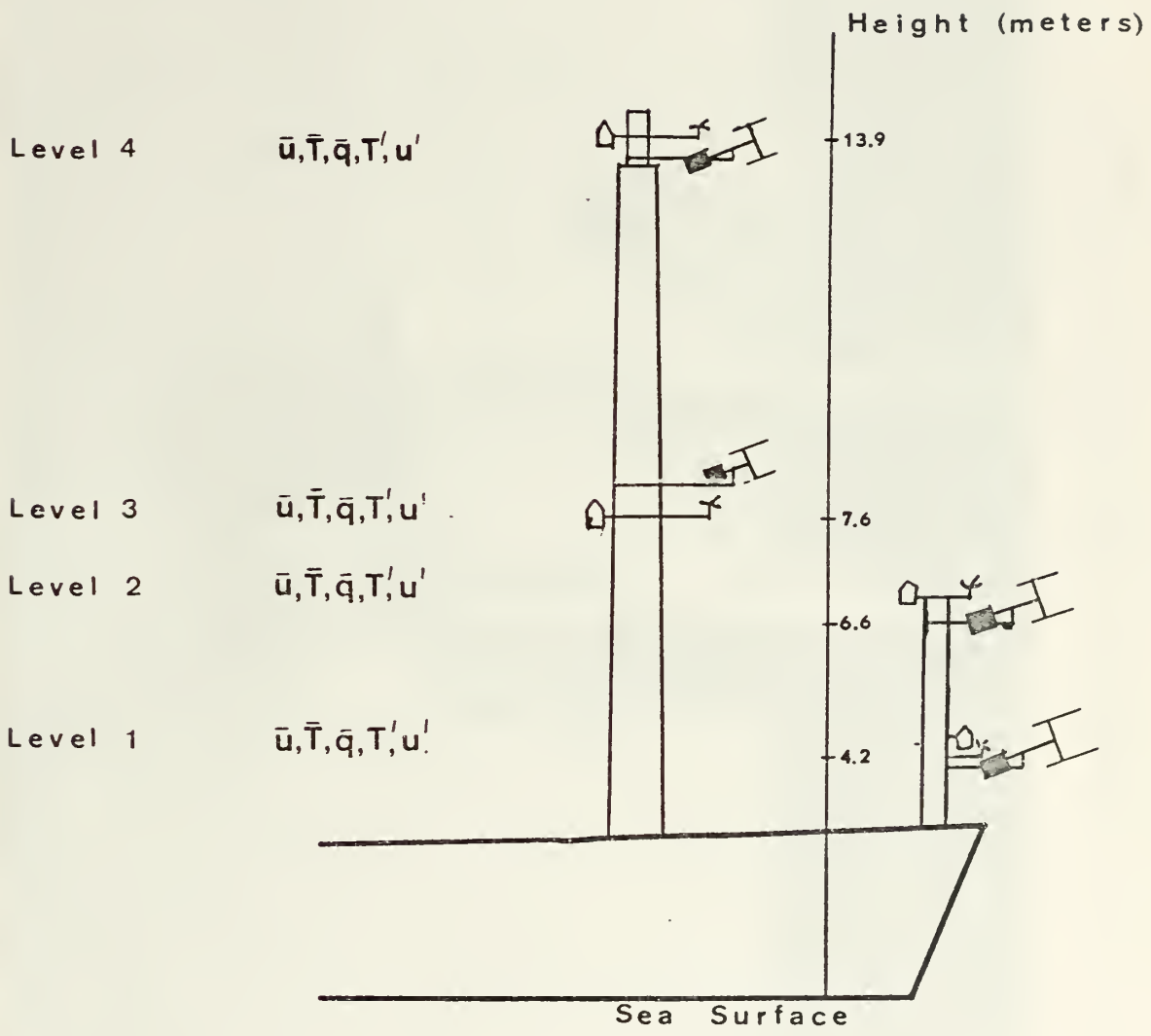

Figure 4. Mounting arrangements.

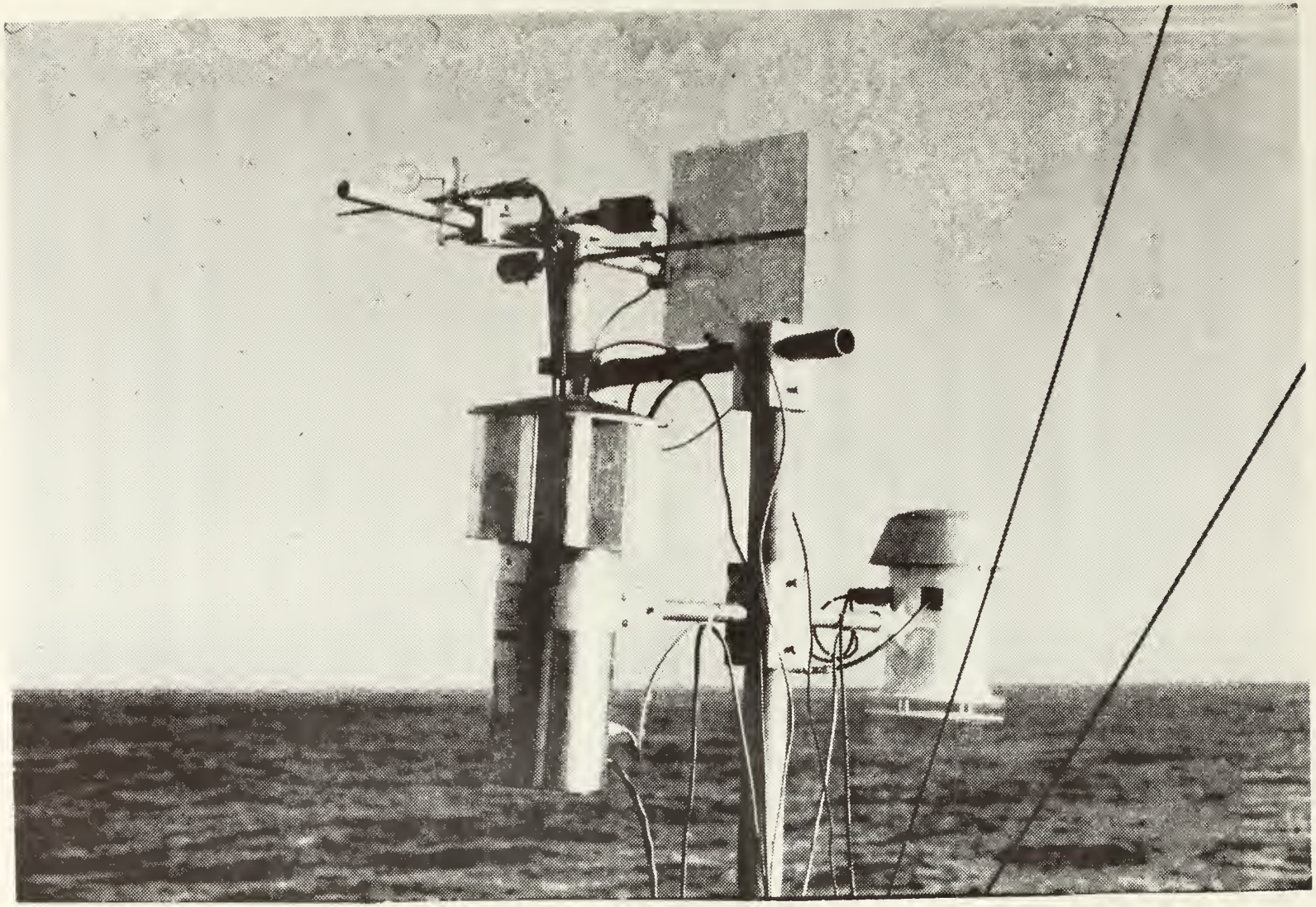

Figure 5. Vane and probe arrangement.

KHz and the variable decade module operated with a 0-60 ohm range. The signal conditioner had a linear frequency response from DC to 400 KHz and permitted voltage suppression in one volt steps from 0-29 volts.

Sensor placement required exceptionally long cables, but any decrease in system frequency response had little effect in the frequency band of interest.

In general the performance of the hot-wire system was excellent throughout the experiments.

Temperature fluctuations were also measured with a TSI Model 1210 configuration using platinum wire sensors. Electronics used were the GTE Sylvania Model 140 thermosonde temperature modules, which can be used to make both single point temperature fluctuation and ΔT measurements. The temperature module is designed for measurements of temperature variations down to $0.001^{o}C$ at frequencies up to 1 KHz.

Mean measurement systems are described in Smedley's (1975) study.

C. SENSOR CALIBRATION

1. Hot Wires Calibration

In-situ calibrations of the velocity sensors were accomplished several times during each experiment. In this procedure, recordings were made of both the cup anemometer RPM count and the corresponding hot wire voltage output. The sensor wind speed and voltage relationship is given by

$$v^2 = a(\bar{u})^{\frac{1}{2}} + b \qquad (17)$$

where v is the voltage and $\bar{u}$ is mean wind speed for a particular level. The constants a and b are calibration curve slope and intercept respectively obtained from the in-situ calibration. Figure 6 is a sample calibration curve constructed from in-situ values in one period.

To convert the power spectral density levels to velocity units required a calibration factor such that

$$c\ v' = u' \tag{18}$$

where c is the calibration factor in $\frac{cm/sec}{volt}$, v' is the voltage flucuation and u' is the velocity fluctuation. Differentiating Equation (17), we get

$$\left(\frac{4v(\bar{u})^{\frac{1}{2}}}{a}\right) v' = u' \tag{19}$$

or

$$c = \frac{4v(\bar{u})^{\frac{1}{2}}}{a} \tag{20}$$

To obtain the calibration factor, c, Equation (17) was initially solved for v using the appropriate sensor level's mean wind speed $\bar{u}$ and also the particular sensor's calibration curve slope and intercept.

2. Platinum Wires Calibration

Wire resistance is related to temperature by the equation

$$R = Ro(1 + \alpha(T - To)) \tag{21}$$

where R = resistance, T = calibration temperature, To = $0^{o}C$, Ro = resistance at To, and α = $.0039/^{o}C$ (temperature coefficient of resistance for platinum). Each wire's

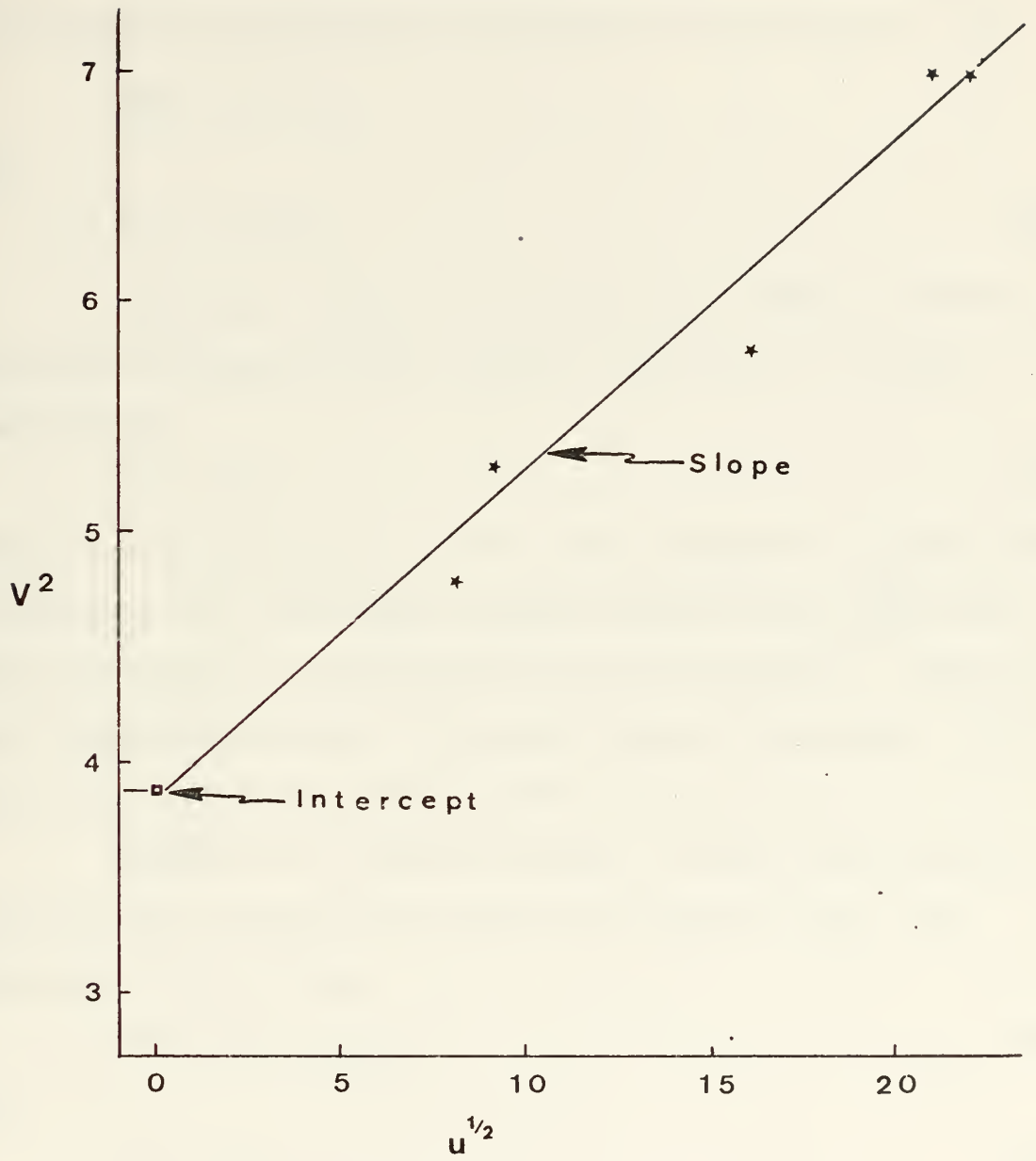

Figure 6. Hot wire calibration plot.

resistance was measured in the laboratory at a temperature T, to determine Ro.

We can relate temperature fluctuations to wire resistance fluctuations by differentiating Equation (21).

$$dR = \alpha \, Ro \, dT$$

or

$$R' = \alpha \, Ro \, T' \tag{22}$$

Recorded voltage fluctuations can then be related to resistance changes by the transfer function, H, in the expression

$$v' = H \, R' \tag{23}$$

where H was determined for the four bridges by varying the resistance of a TSI 1056 Variable Decade Probe Resistance and recording the corresponding voltage changes. Figure 7 is a calibration curve of voltage versus resistance, where the slope determines the transfer function, H.

Finally, to relate recorded voltage fluctuations to temperature fluctuations substitute Equation (23) into Equation (22), giving

$$T' = \left(\frac{1}{H \, \alpha \, Ro} \right) v' \tag{24}$$

or

$$T' = C_H \, v' \tag{25}$$

where C_H is the temperature calibration factor in ^{o}C/volt.

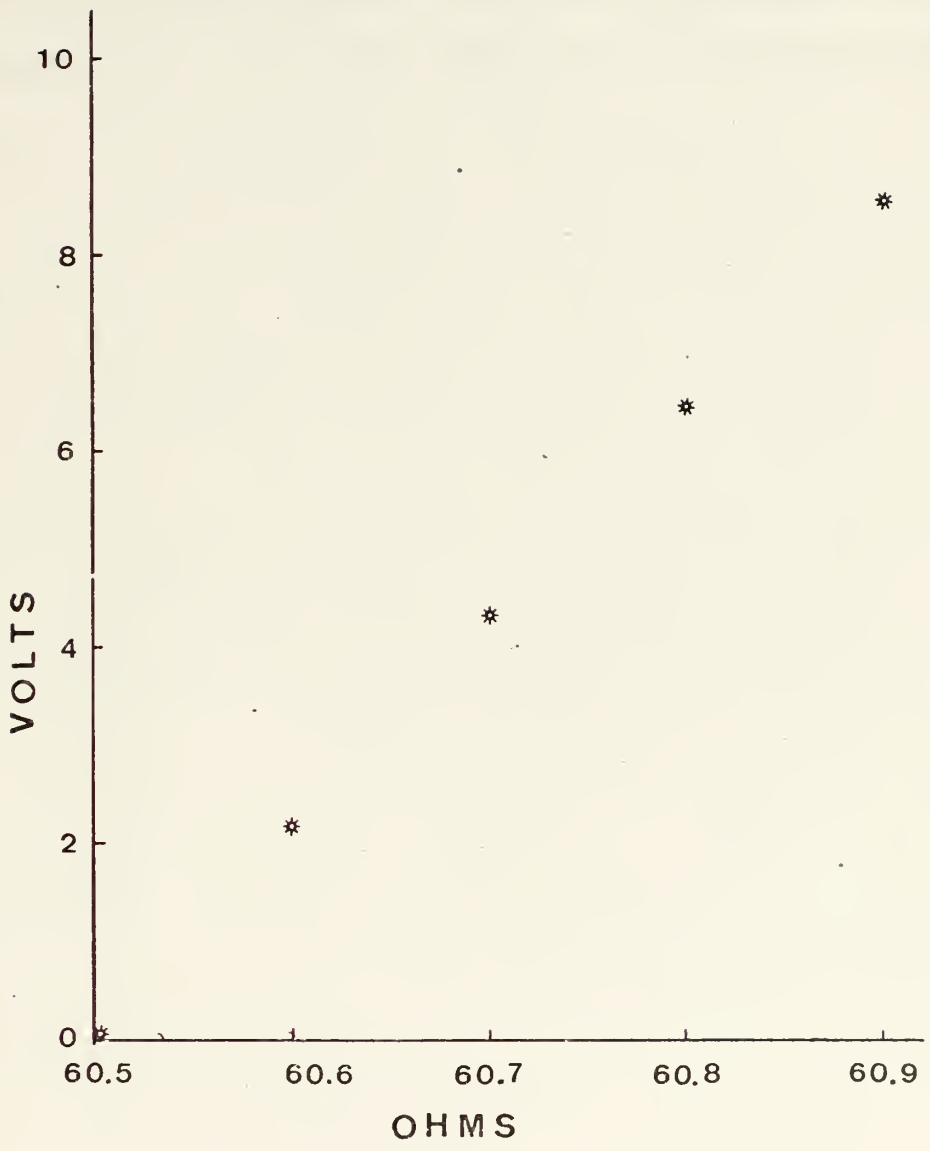

Figure 7. Platinum wire transfer function plot.

D. SIGNAL PROCESSING

The data from the four levels was recorded simultaneously, in analog form, on a 14 channel tape recorder.

The signals were continuously monitored with an oscilloscope and an 8 channel strip chart recorder to insure the quality of the recorded signal and to detect equipment failures.

IV. DATA PROCESSING AND ANALYSIS

A. PRELIMINARY ANALYSIS

Selection of data periods was based on signal evaluations of strip chart records, mentioned in section III.D, and on evaluations of experimental logs of equipment status and ship positioning. Primary consideration was given initially to obtaining 18 minute records with temperature and velocity signals at all levels. This was later changed to 21 minute records due to characteristics of the anolog spectrum analyzer.

B. PROCEDURES

Several procedures were adopted to best handle the turbulence data. These are outlined in Appendix A in detail. All spectral analysis was performed by processing the recorded analog signal on a Federal Scientific Model UA-500-1 Spectrum Analyzer-Averager shown in Figure 8.

The averager output was a logarithmic plot of the power spectral density in $Volts^2/Hz$, versus frequency f in Hz. The plotter was calibrated so that all plots would concide with Bone's (1974) digital plots. Thus, a preliminary visual comparison was made to verify the spectra prior to computations. Figure 9 illustrates a sample of the plot comparison for a data period common to Bone's (1974) study and this study. Figure 10 shows a typically good graphical plot of spectrum versus frequency used in this study. Figure 11 is an example of a poor spectral plot.

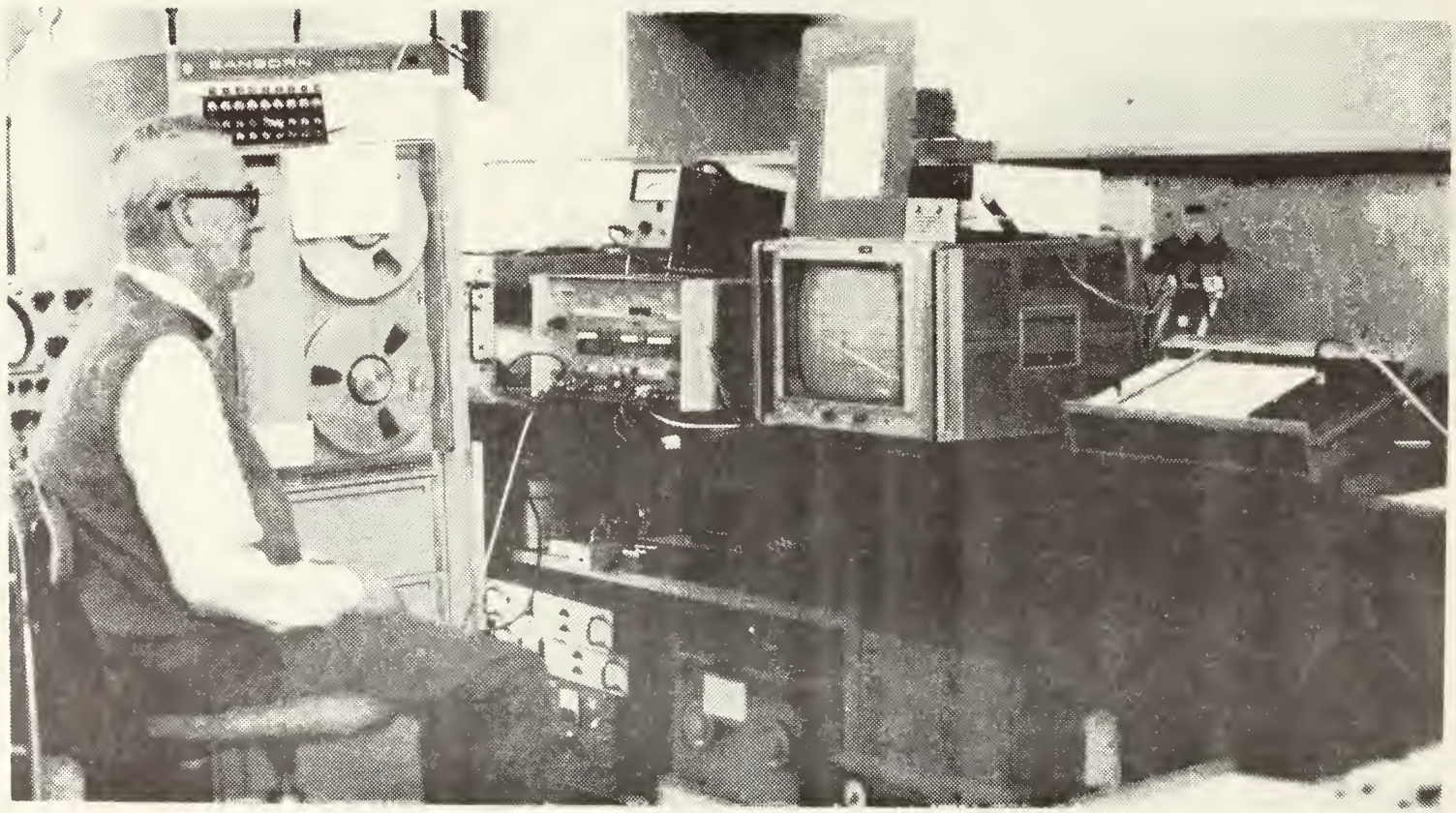

Figure 8. Spectrum analyzer and related equipment.

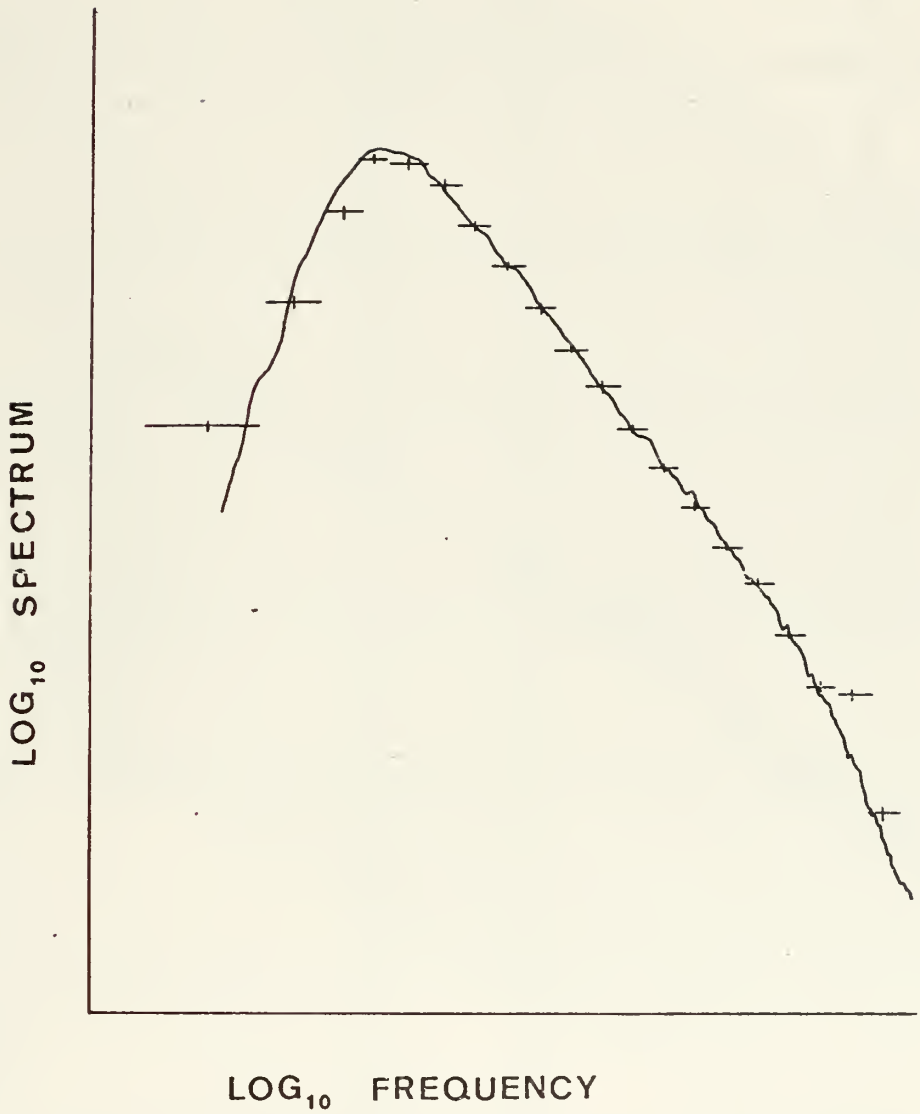

Figure 9. Comparison of digital and spectrum analyzer velocity spectra for 1855-1913L, 18 Jan. 74.

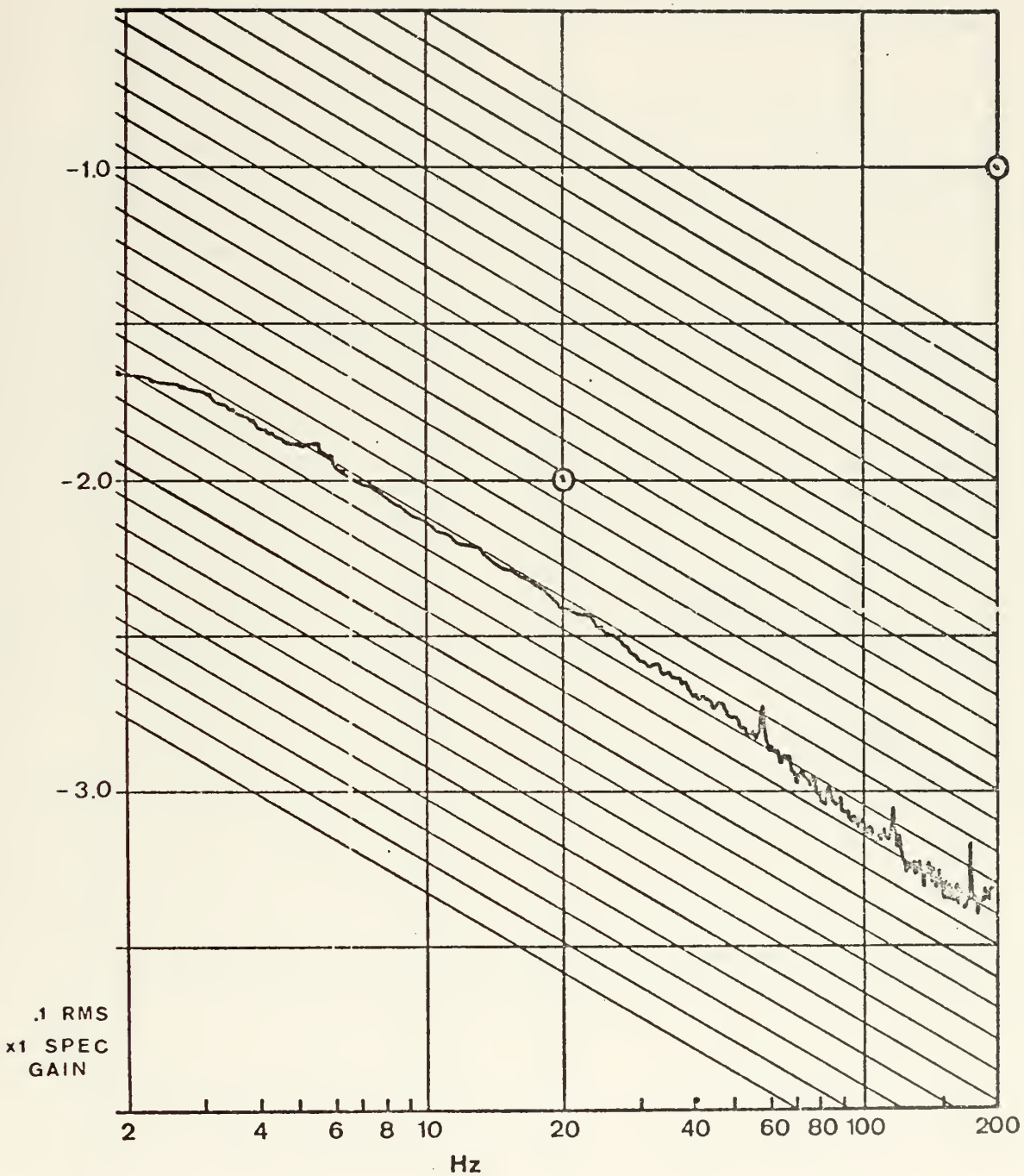

Figure 10. Typical good analyzer spectral plot.

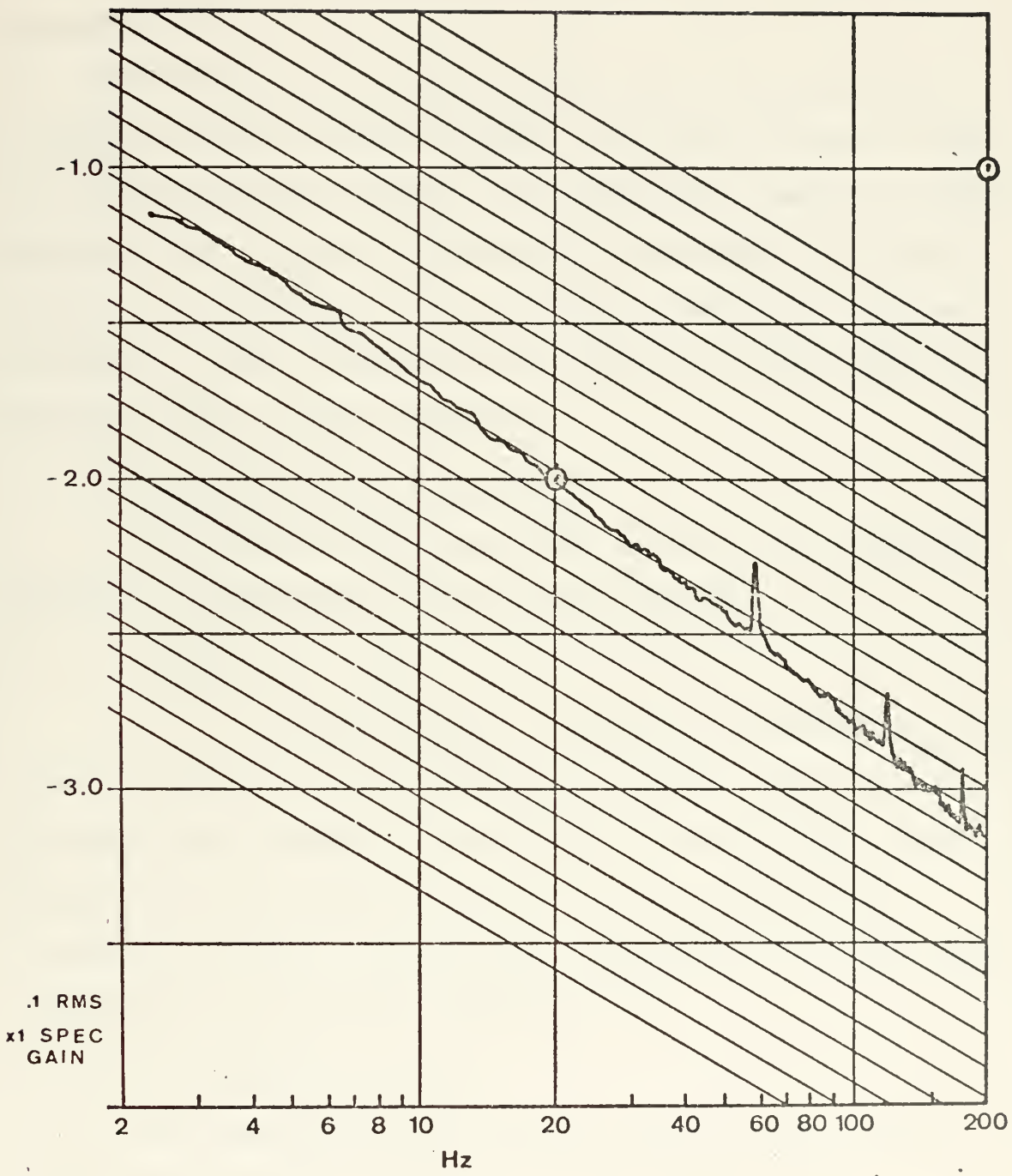

Figure 11. Typical poor analyzer spectral plot.

C. SPECTRAL INTERPRETATION

Scaling of the spectral plot to relate an RMS input voltage to a power per unit of frequency is discussed in Appendix B.

The single point method as previously discussed by Johnston (1974) and Bone (1974), was used to obtain ε and C_T^2 values from the velocity and temperature spectra. Using many spectral points in the inertial subrange (-5/3 slope region), an intercept at an arbitrary frequency f can be obtained. This intercept value yields the power spectral density (PSD), after correction.

1. Determination of ε and u_*

The measured PSD value was converted to a spectral density in engineering units by the equation

$$\phi(f) = c^2 \cdot \text{PSD}$$

$$= (\text{cm/sec}/_{\text{volt}})^2 \cdot \text{volt}^2/_{\text{Hz}} = (\text{cm/sec})^2/_{\text{Hz}} \quad (26)$$

where c is the hot-wire calibration factor. The solution to Equation (15) yielded a value for ε at each level. Then, Equation (4) and (6) were solved for a u_* value and a corrected u_* value respectively. Corrected u_* values were not valid for Richardson numbers > 0.2.

2. Determination of C_T^2

The following equation was used to convert PSD values from measured spectra to dimensional values

$$\phi_T(f) = C_H^2 \cdot \text{PSD}$$

$$= (^{\text{o}}\text{C}/_{\text{volt}})^2 \cdot \text{Volt}^2/_{\text{Hz}} = {}^{\text{o}}\text{C}^2/_{\text{Hz}} \quad (27)$$

where C_H is the calibration factor for the temperature system. Solving Equation (16) for C_T^2 yielded a value for each level Z. These values were then applied to Equation (12) to obtain C_N^2 for possible comparison with optically derived C_N^2 values.

V. RESULTS

A. DATA PERIODS EXAMINED

Fluctuating velocity, u', and temperature, T', data were studied for the nine periods shown in Table I. Four levels of both velocity and temperature were desired, but temperature signals were not always available for all levels due to various component failures. Table I summarizes the periods examined and what data was available for each period.

B. VELOCITY SPECTRAL RESULTS

For seven of nine periods studied, four levels of velocity, u', were available. Equation (15) was used to calculate ε from values at each level from selected frequencies, f, spectral densities, $\phi(f)$, and wind speed, $\bar{u}$. Each computed value ε was then used in Equations (4) and (6) to determine a value for the friction velocity, u_*.

Table II summarizes the ε and u_* results along with stability corrected values of u_*, profile u_* estimates obtained by Smedley (1975), and Richardson numbers, R_i. Most spectra exhibited the -5/3 slopes for the inertial subrange region which validates the method used to determine ε from the spectral densities. Except for one value on March 27, u_* values are all less than 0.5 m/sec^{-1} and most are in the expected range of 0.1 - 0.5. Most periods of u_* seem to reflect the constant flux theory accurately, especially if

TABLE I

DATA PERIODS IN THIS STUDY

PERIOD	DATE	TIME	LEVEL	PARAMETER
1	27 Mar. 74	1841-1902L	1	T'
			2	u', T'
			3	u', T'
			4	u'
2	27 Mar. 74	1902-1923L	1	u', T'
			2	u', T'
			3	u', T'
			4	u'
3	27 Mar. 74	1928-1945L	1	u', T'
			2	u', T'
			3	u', T'
			4	u', T'
4	27 Mar. 74	2117-2138L	1	u', T'
			2	u', T'
			3	
			4	u', T'
5	28 Mar. 74	1902-1923	1	u', T'
			2	u'
			3	u', T'
			4	u', T'
6	28 Mar. 74	2059-2117L	1	u', T'
			2	u', T'
			3	u'
			4	u', T'
7	18 Sept. 74	1643-1701L	1	u', T'
			2	u', T'
			3	u'
			4	u', T'
8	19 Sept. 74	1735-1753L	1	u', T'
			2	u', T'
			3	u'
			4	u', T'
9	19 Sept. 74	1900-1918L	1	u', T'
			2	u', T'
			3	u'
			4	u', T'

TABLE II

ε and u_* Results

HEIGHT (m)	ε (m^2-sec^{-3})	u_*[1] (m-sec^{-1})	u_*[2] (corrected)	u_* (profile)	R_i
Period 1	27 March 74		1841-1902L		
6.6	.0061	.25	*	.15	.53
7.6	.0069	.27	*		.62
13.8	.0069	.33	*		.43
Period 2	27 March 74		1902-1923L		
4.1	.021	.32	.29	.25	.06
6.6	.012	.31	.19		.14
7.6	.019	.38	.28		.16
13.8	.013	.41	*		.38
Period 3	27 March 74		1928-1945L		
4.1	.240	.72	.65	.26	.06
6.6	.039	.46	.34		.13
7.6	.018	.37	.25		.15
13.8	.021	.48	*		.35
Period 4	27 March 74		2117-2138L		
4.1	.044	.41	.34	.39	.09
6.6	.025	.40	.36		.06
13.8	.016	.44	.25		.17
Period 5	28 March 74		1902-1923L		
4.1	.039	.40	.38	.30	.02
6.6	.0030	.20	.18		.05
7.6	.0030	.20	.19		.05
13.8	.0013	.19	.14		.13

NOTE

[1] computed from equation 15

[2] computed from equation 6

* no data

TABLE II (continued)

HEIGHT	ε	u_*	u_* (corr.)	u_* (profile)	R_i
Period 6	28 March 74		2059-2117L		
4.1	.020	.32	.27	.17	.09
6.6	.013	.32	.14		.19
7.6	.010	.31	*		.22
13.8	.011	.38	*		.52
Period 7	18 September 74		1643-1701L		
4.1	.0089	.24	.19	.10	.12
6.6	.0015	.16	*		.22
7.6	.00049	.11	*		.26
13.8	.019	.46	*		.62
Period 8	19 September 74		1735-1753L		
4.1	.0099	.25	.26	.16	-.11
6.6	.0063	.25	.26		-.23
7.6	.0017	.17	.17		-.27
13.8	.0039	.27	.26		-.64
Period 9	19 September 74		1900-1918L		
4.1	.0077	.23	.24	.25	-.04
6.6	.0076	.27	.28		-.08
7.6	.0013	.15	.16		-.09
13.8	.045	.62	.64		-.22

obviously bad levels are discarded in the periods. Those results which prevent nearly the same u_* flux for all levels in a period, were readily attributed to a departure from the -5/3 spectral slope. A comparison of this study's u_* and stability corrected u_* values with Smedley's regression u_* values, provides close agreement for at least two levels for each period. The comparatively high u_* values for level 4 in the stable cases has not been explained, but it also occurred in one of the two unstable cases.

Figure 12 is a typical plot of height versus ε for a stable case. It shows close agreement with the -1 slope expected for the near neutral case, according to Equation (5). Figure 13 illustrates the unstable case. Here again we have agreement with the neutral case -1 slope, except for level 3. Poor results for level 3, in this case, can be related to a poor spectral plot with insufficient amplitude and a slight departure from a -5/3 slope. This deviation is not expected since level 2 and 3 are within one meter in height.

Composites of height versus ε for all periods are shown in Figure 14 for stable and unstable cases. Obviously bad data was not included in these composites. Both the stable and unstable cases show close agreement to the near neutral prediction. This differs from the previous results of Bone (1974), in that his slopes deviated from the -1 value, as expected for non-neutral conditions.

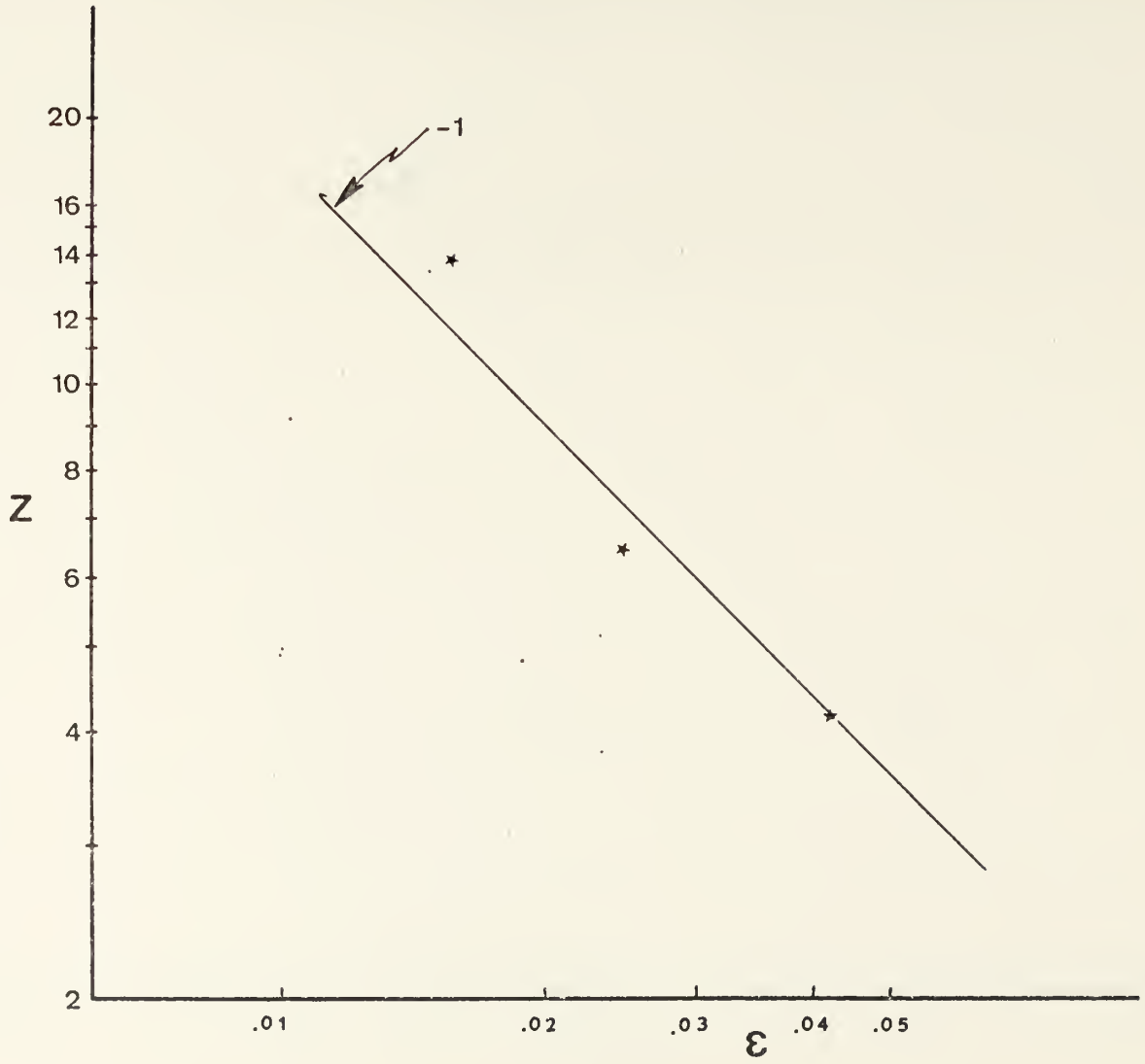

Figure 12. Typical plot of height vs. ε; stable case.

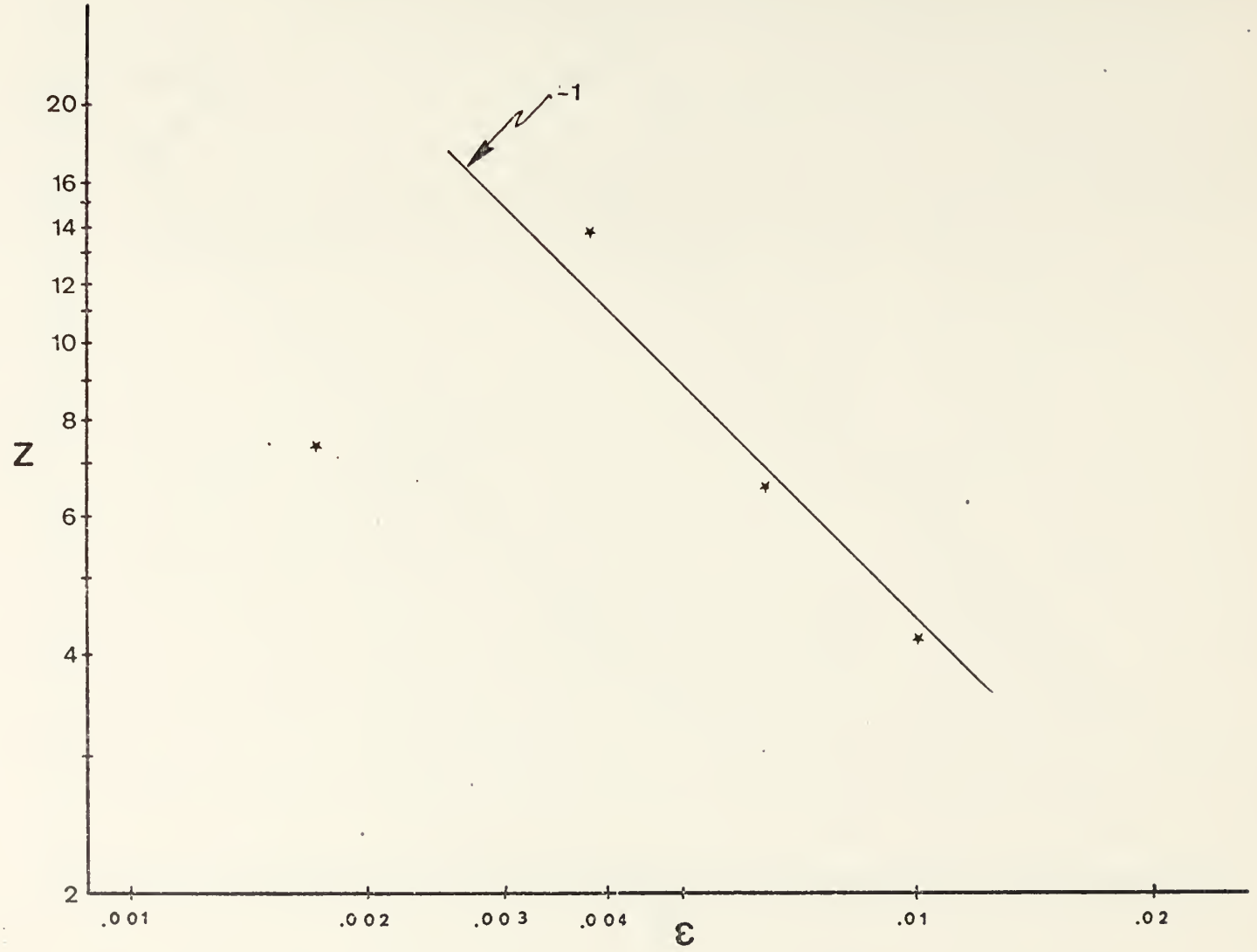

Figure 13. Typical plot of height vs. ε; unstable case.

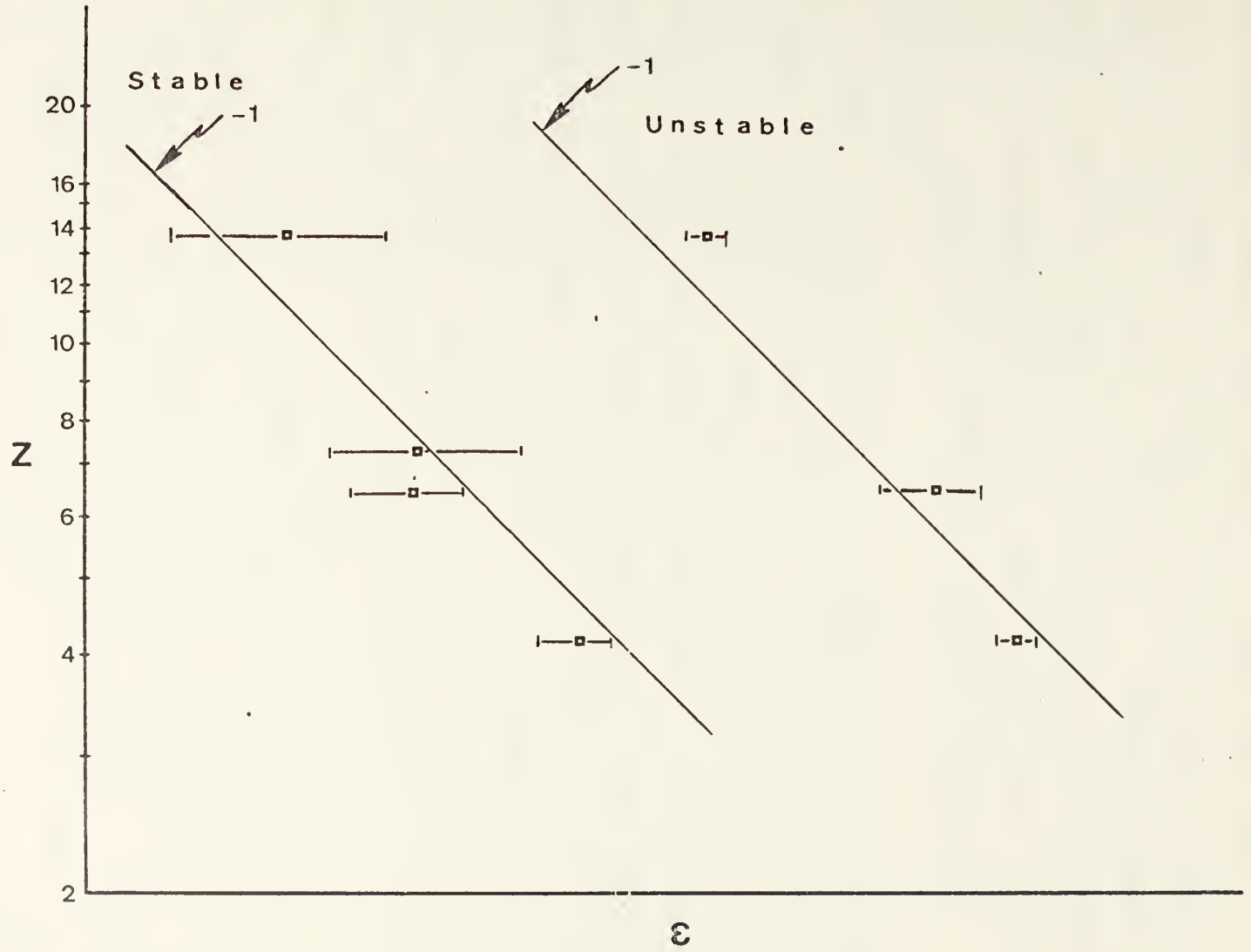

Figure 14. Composite plot of height vs. ε; periods 1-9

C. TEMPERATURE SPECTRAL RESULTS

One period had four levels of temperature, T', data, while eight periods only had three levels of T' data. C_T^2 values were computed by applying Equation (16) to values at each level for selected frequencies, f, spectral densities, $\phi_T(f)$, and wind speeds, $\bar{u}$. Equation (12) was then applied to the resultant C_T^2 to get C_N^2. The C_N^2 values will be used by investigations into coincident optical propogation experiments.

Table III is a summary of the C_T^2 and C_N^2 results for this study. It also includes Smedley's (1975) profile values of C_T^2 for a comparison. The height variations of C_T^2 in the stable periods were generally consistent with predictions. During unstable periods there appeared to be some lack of consistency between levels. Here again, most inconsistencies were traced back to a poor spectra. C_T^2 values which are within an order of magnitude of Smedley's results are considered a fair correlation. Such correlation does not occur for any level in periods 1, 4, and 7.

A typical plot of height versus C_T^2 for the stable case is shown in Figure 15. It agrees very well with the expected -3/2 slope. The unstable case is shown in Figure 16. The expected slope of -3/4 for height versus C_T^2 agrees reasonably well with two of the three data points. The 4 meter level point can be attributed to a spectra with a slope greater than -5/3 along with comparatively small amplitudes.

TABLE III

C_T^2 and C_N^2 Results

HEIGHT (m)	C_T^2 [1] ($^oC^2\ m^{-2/3}$)	C_T^2 [2] (profile)	C_N^2 ($m^{-2/3} x10^{-14}$)	R_i
Period 1	27 March 74		1841-1902L	
4.1	.0017	*	.16	.25
6.6	.0034	*	.32	.53
7.6	.0034	*	.33	.62
Period 2	27 March 74		1902-1923L	
4.1	.0021	.043	.20	.06
6.6	.0022	.0061	.21	.14
7.6	.0043	.0032	.42	.16
Period 3	27 March 74		1928-1945L	
4.1	.0057	.042	.55	.06
6.6	.0050	.0065	.48	.13
7.6	.0062	.0036	.60	.15
13.8	.0015	*	.14	.35
Period 4	27 March 74		2117-2138L	
4.1	.0036	.072	.35	.09
6.6	.0032	.020	.31	.06
13.8	.0018	.00089	.17	.17
Period 5	28 March 74		1902-1923L	
4.1	.017	.016	1.7	.02
7.6	.026	.0040	2.6	.05
13.8	.0018	.00055	.18	.13

[1] value computed from Equation (16)

[2] values from Smedley (1975)

* profile unavailable, R_i >.20

TABLE III (continued)

HEIGHT	C_T^2	C_T^2 (profile)	C_N^2	R_i
Period 6	28 March 74		2059-2117L	
4.19	.060	.014	5.9	.09
7.64	.030	.0046	3.0	.19
13.89	.024	*	2.3	.52
Period 7	18 September 74		1643-1701L	
4.19	.00030	.0016	.029	.12
6.6	.00016	.0012	.015	.27
13.89	.00014	*	.013	.68
Period 8	19 September 74		1735-1753L	
4.19	.00050	.0063	.048	-.11
6.6	.0025	.0031	.24	-.23
13.89	.00069	.0015	.07	-.64
Period 9	19 September 74		1900-1918L	
4.19	.00062	.0081	.059	-.04
6.6	.0019	.0036	.18	-.08
13.89	.0011	.0016	.11	-.09

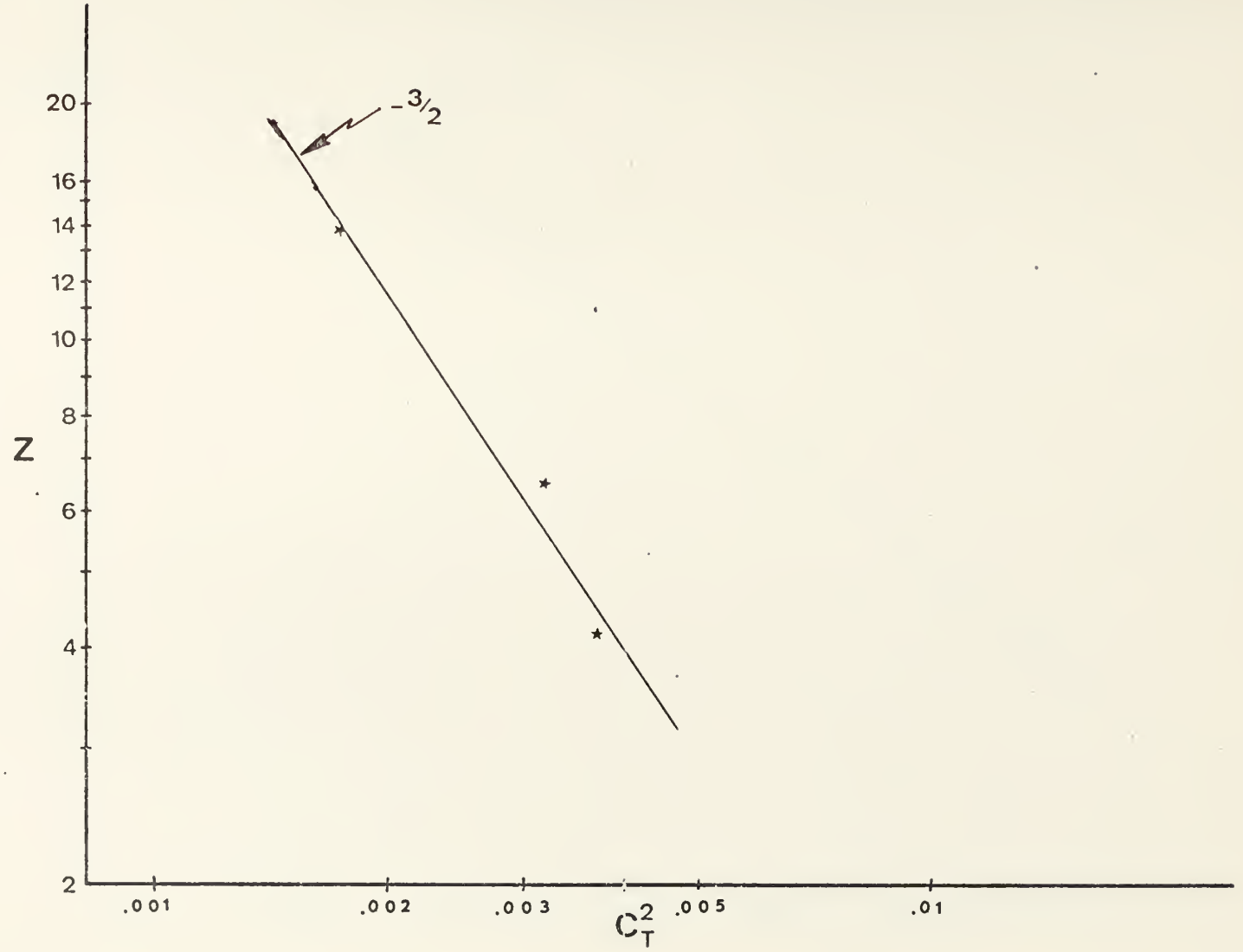

Figure 15. Typical plot of height vs, C_T^2; stable case.

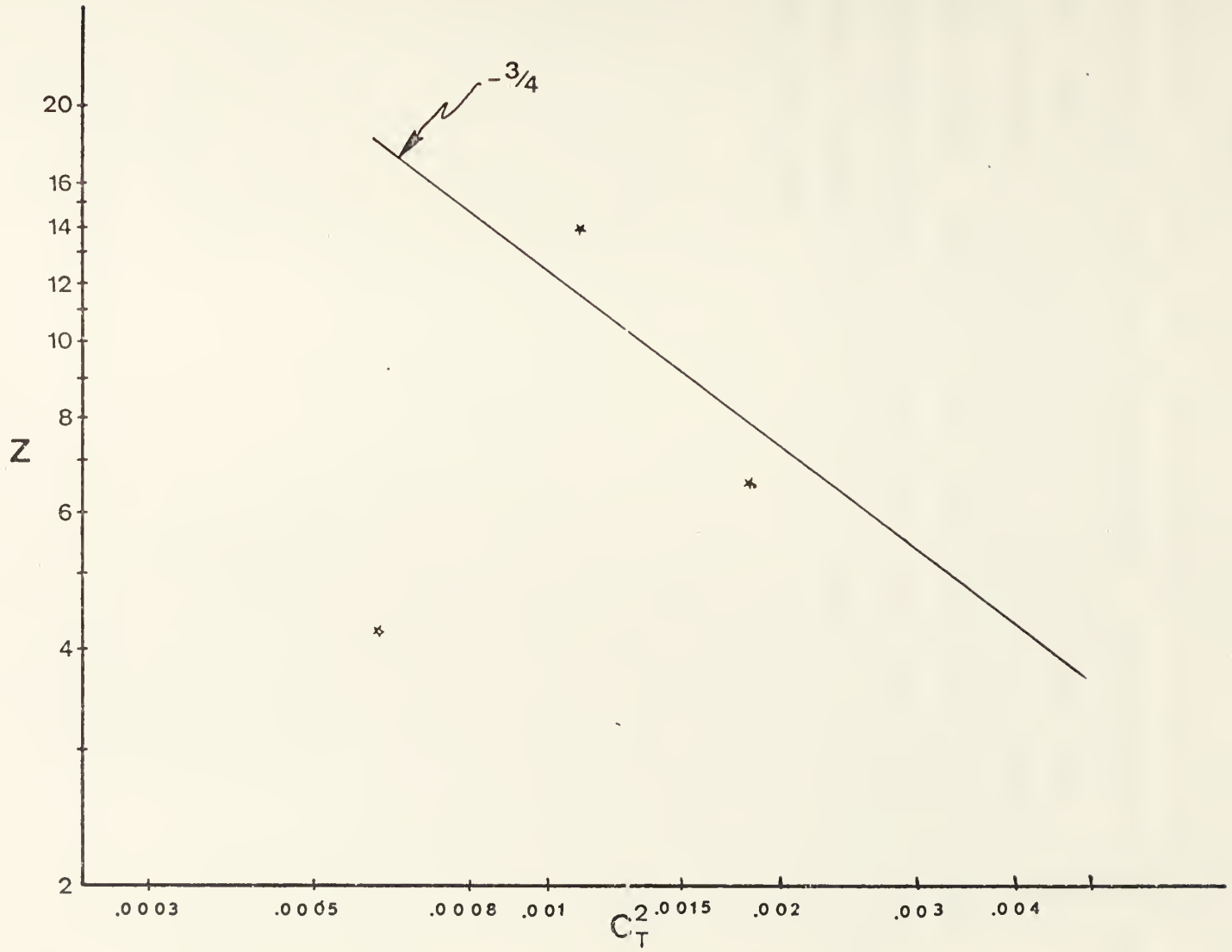

Figure 16, Typical plot of height vs, C_T^2; unstable case

Figure 17 includes composites of height versus C_T^2 for all periods for both the stable and unstable cases. For these composites, obviously unrepresentative data were not plotted. In the stable case, agreement with an expected slope greater than -3/2 is possible. The lowest level shows the greatest range in relation to the slope line. This is attributed to a comparatively weak amplitude spectra in many cases. Actually, this level should have the largest amplitude spectra in comparison to the other three levels. There is good agreement with the expected -3/4 slope for the unstable case.

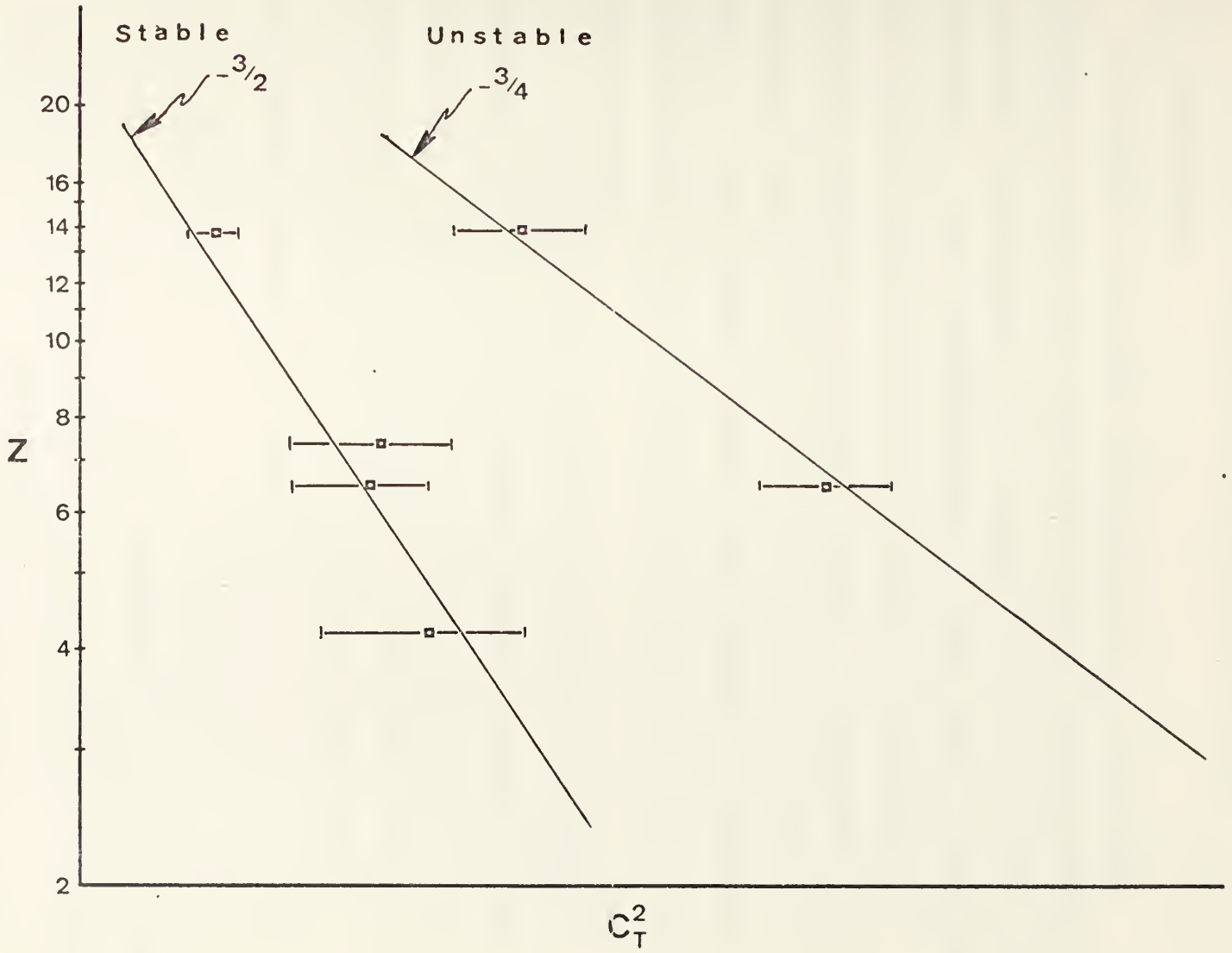

Figure 17. Composite plot of height vs. C_T^2; periods 1-9.

VI. CONCLUSIONS AND RECOMMENDATIONS

A. CONCLUSIONS

In general, the height variations of ε, u_* and C_T^2 observed in this study agree with the overland expressions developed by Wyngaard. The agreement with the constant flux assumption is an important result of this study. Most deviations from expected results were able to be attributed to apparent anomalies in spectral results. Correlation of C_T^2 results with Richardson number derived C_T^2 values was not good. However, since spectral results were generally consistent between levels, the spectral results are considered to be more reliable.

It has been shown that the analog spectral analysis performed in this study produced information which is as reliable as that from digital methods. Application of the analog method on the large amount of available data should furnish information as to the reasons for identified departures from expected results.

B. RECOMMENDATIONS

Future experiments would be improved by relocating level 3 further up the mast, say to 10 meters, to obtain a greater separation between levels 2 and 3.

Improved strip chart monitoring of u' and T' signals during experiments is needed. Improved monitoring of these

records during the experiment could reveal anomalous signal levels and corrections during the experiment could be accomplished. In general, a decrease with height of both u' and T' signals is expected.

More frequent in-situ calibrations of the hot wire anemometers should be made to increase the accuracy of results, especially for experiments of long duration. Frequent resistance measurements, on the platinum wires during the experiments is also necessary for this purpose.

Finally, it is recommended that the spectrum analyzer's "vernier" input amplitude control be tested on a few poor periods to determine if the analyzer sensitivity could be part of the problem in the lack of consistency between some levels. Readjustment for each level and also obtaining a spectral amplitude calibration plot, would result in maximum sensitivity and minimum distortion of the spectral output. A.C. harmonics from the ships power supply should also be filtered out to prevent spectral distortion.

APPENDIX A

A. SPECTRUM ANALYZER-AVERAGER

1. General

The following discussion is for further amplification of the spectral analysis procedures used in reducing all data for this study and will serve to aid those who will continue to study turbulence data in the same manner.

2. Equipment

All spectrum analysis was performed by using a Federal Scientific Model UA-500-1 Spectrum Analyzer-Averager, which is a time-compression spectrum analyzer, using a digital speed up loop.

In time-compression spectrum analyzers, the input data is digitized and stored in a memory. While the memory is being updated with new data, its contents are read out repeatedly at a very high rate. The speeded-up high frequency replica of the analog input signal is spectrum-analyzed, using a wide filter which is being stepped rapidly in real time.

A recorder analog input signal is converted to digital after passing through an anti-aliasing low-pass filter. The sampling frequency is controlled by the analyzer frequency operating range. The digital signal is stored in a 1500 word digital memory, circulates in the memory, and can be non-destructively read out at an accelerated rate. This memory output is then put through a digital to analog converter.

The converter output is a time-compressed, accelerated form of the original analog input signal. It passes through a heterodyner and is applied to a stable crystal filter, causing the filter to observe successive frequency-resolution cells. A weighting function modifies the analyzer's frequency selectivity. Settling time of the crystal filter is short enough to obtain one spectral point each time the memory does one recirculation. Five hundred spectral points can be obtained in 50 milliseconds. Averaging of the spectral wave form is then accomplished with a digital ensemble averager to obtain statistical stability in mean spectral characteristics. The final result in storage is a real-time power-spectral-density (PSD) representation available at output terminals. The averager has two 500 word memories.

A Hewlett-Packard X-Y Plotter was used to obtain a hard copy of results for each sampling period.

3. Operating Procedures

a. Analysis Range

The range considered best for this study was 200 Hz for all data analyzed. This resulted in a sample interval of 2.5 seconds (memory time). Since the highest frequency of interest was about 100 Hz, the Nyquist sampling theorem was satisfied. The sampling rate for the above analysis range is 600 Hz, with a filter bandwidth of 0.4 Hz. 100 percent of the input data is processed for the 200 Hz analysis range.

b. Input Mode

Input signal coupling was used in the AC mode to analyze only the AC component of the input signal. Hence, the analysis was not subject to DC offsets. This mode has a low-frequency 3-dB cutoff at less than 3 Hz. A presampling filter provides at least 50 dB of attenuation per octave fall off (i.e. 50 dB at 400 Hz). This filter and a sampling rate of three times the analysis range eliminate aliasing.

c. Input Amplitude

The input amplitude was adjusted for varying values of the RMS input voltage to attenuate the level of the input signal. The Vernier Cal. control was left in the detent position so that the input amplitude switch was functional from 0-dB through -40-dB, in 10-dB steps only. An RMS voltmeter was used to monitor sample portions of the input analog signal to determine a volts RMS full scale. The input amplitude was then adjusted for a volt setting so that full scale indications didn't exceed this volt setting. Periodic noise spikes were not considered. Overflow indications were not normally excessive if this procedure was followed. This indicator may flash a few times per second without danger of significant signal distortion.

d. Transient Capture Controls

Depression of the manual button, with the hold light off, enabled the memory to accept new data continuously. The two other available modes were not used in this analysis. Then the trigger polarity and sensitivity controls and the

transient auto delay switches are not functional. The external sampling switch must also be off.

e. Output Spectrum Gain

Pushbutton operation introduces a gain (0 dB, +10 dB, + 20 dB) to the analyzer output prior to averaging of spectra. Operation, for this study, was in the +10 dB (gain x 3.2) mode, due to the characteristics of the data signals. The output gain overload light indicates when spectral peaks are above full scale and are clipped. This occurred infrequently.

f. Amplitude and Frequency LIN/LOG Switches

Logarithmic scale for both amplitude and frequency were used for all spectra.

g. Display Sweep Controls

The FAST OSCILL mode must be used for the averaging of a signal and the SLOW PLOT mode should be selected for plotting the memory contents of the X-Y plotter. The START, STOP, RESET pushbuttons control the averaging or plot mode elected. In slow plot an automatic rate control is used for large signal excursions to avoid plotter slew-rate problems.

h. Averager

(1) Active Memory Control. This switch selects that memory where averaging takes place and whose contents are displayed or plotted. The ERASE pushbutton will erase the selected memory if FAST OSCILL is selected.

(2) Averaging Method Controls. In the SUM mode, each non-redundant analyzer spectrum is added to previous

spectra stored in the active memory. The INSTANT SPECT control can't be depressed when an averaging process is to be started.

(3) Average Stop Mode Controls. The manual mode was used in this study to stop each analysis at 18 minutes with the STOP control. The Number of Spectra-N switch then functioned as a gain control if set at N less than 256. This proved to be a problem, in that the analyzer looks at this switch to indicate how many samples are coming. If the number N selected and the number N of samples do not coincide when analysis stops, then the spectra is not complete. There is no problem in the Stop-At-N mode.

i. Calibration

All other operating procedures and the calibration procedures of Analyzer-Averager and displays can be obtained from the manufacturer's instruction manual.

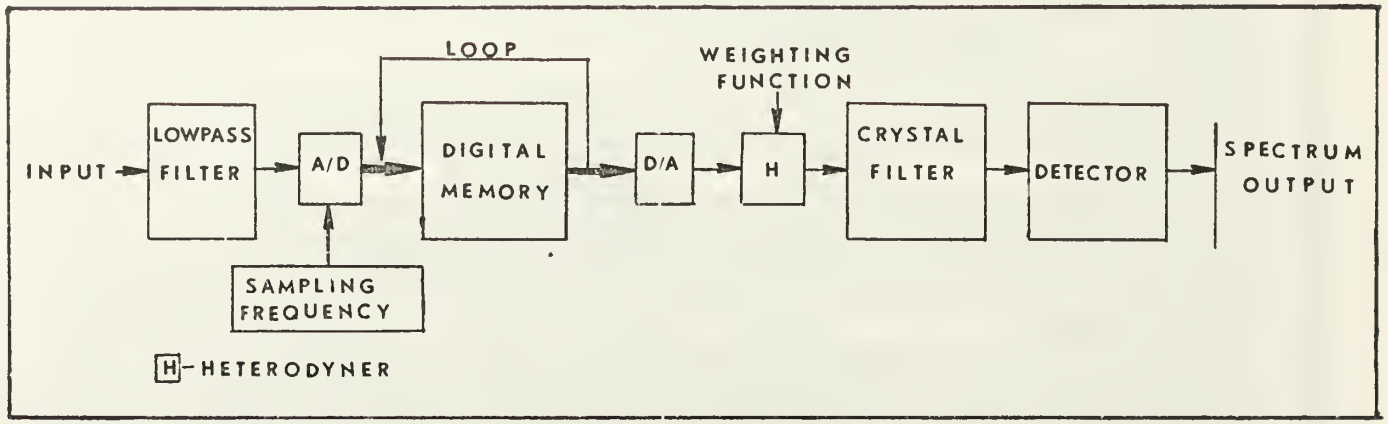

Figure A.1. Block diagram of analyzer-averager.

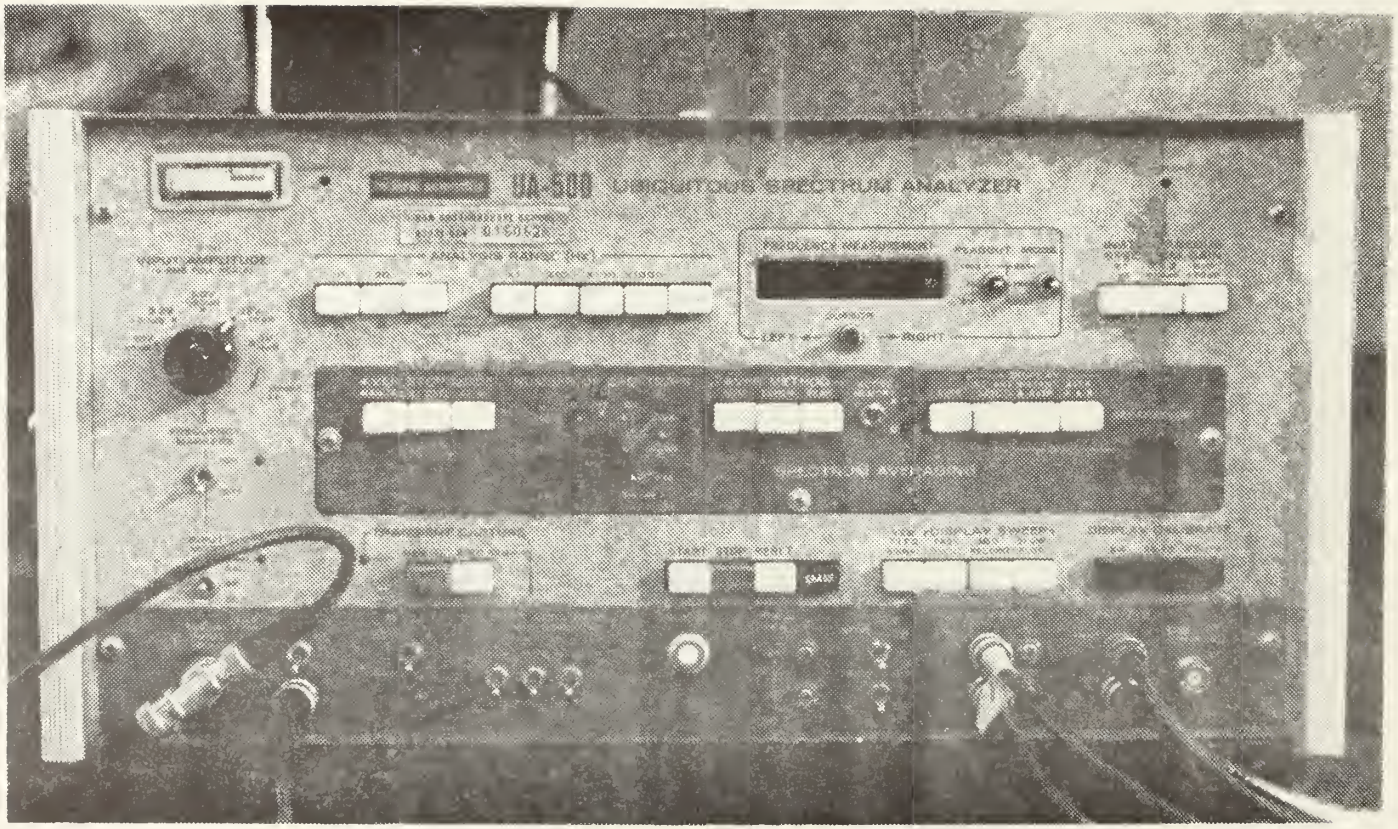

Figure A.2. Federal Scientific Model UA-500-1 Spectrum Analyzer-Averager

APPENDIX B

A. SPECTRAL X-Y PLOT SCALING PROCEDURES

To obtain a power spectral density level, corresponding to an RMS voltage input, a calibrated scale overlay had to be constructed for use in spectral interpretation.

Amplitude scaling was accomplished by an internally generated signal available in the AMPL, CAL input mode, When 0-dB (.1v) input gain was selected, a cal signal with amplitude approximately equal to 0,1 volts RMS appears on the display as a spike at 100 Hz indicating full scale amplitude. This spike was then plotted in the X-Y plotter, along with bench marks, using a spectral gain of 0dB (x1) setting. Successively, the input gain was stepped to attenuate the amplitude of the spike by 10 dB, and a plot of the height of each spike was obtained on the X-Y plot. This plot now represented a graduation of RMS input from a minimum of 0.001 volts to 0.1 volts maximum. These voltages were then converted to LOG 10 and a graduated scale was constructed to that the LOG 10 of volts RMS could be interpolated from a spectral plot. The amplitude scale was adjusted for each spectrum as a function of input attenuation and spectrum gain. These LOG 10 values were then converted to PSD levels for use in calculating epsilon and structure parameter values. The Federal Scientific Manual's equation to convert to PSD is

$$\text{PSD level } (V^2/_{Hz}) = \frac{0.79 \text{ (cal. level } V_{RMS})^2}{\text{Filter Bandwidth}}$$

where the filter bandwidth ($\beta = 0.4$) is a function of the analysis range selected.

LIST OF REFERENCES

1. Bone, T.C., 1974: Small Scale Properties in the Marine Boundary Layer. M.S. Thesis, Naval Postgraduate School, Monterey, California, 70 pp.

2. Garratt, J.R., 1972: Studies of Turbulence in the Surface Layer Over Water (Lough Neagh). Part II. Production and Dissipation of Velocity and Temperature Fluctuations. Quart. J., Roy. Meteor. Soc., 98, 642-657.

3. Johnston, W.E., 1974: Estimating Boundary Layer Fluxes from Shipboard Measurements of Dissipation of Turbulent Kinetic Energy and Temperature Variance. M.S. Thesis, Naval Postgraduate School, Monterey, California, 131 pp.

4. Smedley, G.W. III, 1975: Investigation of Vertical Profiles of Mean Temperature, Wind and Humidity. M.S. Thesis, Naval Postgraduate School, Monterey, California.

5. Taylor, G.I., 1938: The Spectrum of Turbulence. Proc. Roy. Soc., A164, 476.

6. Wyngaard, J.C., Izumi, U., and Collins, S.A., 1971: Behavior of the Refractive-Index-Structure-Parameter near the Ground. Journal of the Optical Society of America, vol. 61, no. 12, 1646-1650.

INITIAL DISTRIBUTION LIST

		No. Copies
1.	Defense Documentation Center Cameron Station Alexandria, Virginia 22314	2
2.	Library (Code 0212) Naval Postgraduate School Monterey, California 93940	2
3.	Naval Oceanographic Office Library (Code 3330) Washington, D.C. 20373	1
4.	Commander, Naval Weather Service Command Naval Weather Service Headquarters Washington Navy Yard Washington, D.C. 20374	1
5.	Professor Kenneth L. Davidson, Code 51Ds Department of Meteorology Naval Postgraduate School Monterey, California 93940	13
6.	Professor Thomas M. Houlihan, Code 59Hm Department of Mechanical Engineering Naval Postgraduate School Monterey, California 93940	3
7.	Mr. P. Vial, Code 048 Naval Ordnance Laboratory White Oak Silver Spring, Maryland 20910	1
8.	Mr. B. Katz, Code 213 Naval Ordnance Laboratory White Oak Silver Spring, Maryland 20910	1
9.	Lieutenant Allan B. Lund Naval Weather Service Facility Fleet Post Office Seattle, Washington 98762	1
10.	Mr. Steve Rinard, Code 51Sr Department of Meteorology Naval Postgraduate School Monterey, California 93940	1

11.	Professor Dale F. Leipper, Code 58Lr Chairman, Department of Oceanography Naval Postgraduate School Monterey, California 93940	1
12.	R/V ACANIA Department of Oceanograpy Naval Postgraduate School Monterey, California 93940	1
13.	Dr. P. Livingston Applied Optics Branch, Bldg. 30 Naval Research Laboratory Washington, D. C.	1
14.	Lieutenant Grant W. Smedley III U.S.S. Dominant (MSO 431) Bayboro Harbor St. Petersburg, Florida 33701	1

Thesis
L896
c.1
160686
Lund
Spectral estimates of
marine turbulence data.